DOI: https://doi.org/10.14311/TPFM.2025.010

VISUALIZATION OF DANTEC 55P11 HOT-WIRE PROBES UNDER AN ELECTRON MICROSCOPE

E. Flídr [1], A. Flídrová [2]

[1] **VZLÚ - Czech Aerospace Research Centre, Beranových 130, 199 05 Prague - Letňany, Czech Republic**
[2] **LASAK s.r.o. Českobrodská 1047/46, 190 00 Prague - Hloubětín**

Abstract

This paper investigates the geometry of hot-wire anemometers using electron microscopy to establish the dimensions of six Dantec single-wire probes (55P11). Measurements were conducted on photographs using a simple in house Python script. The obtained dimensions were then applied in theoretical calculations of the temperature distribution along the wires to demonstrate the significance of accurate probe geometry determination.

Keywords: Hot-wire probes, electron microscopy, dimension measurement.

1 Introduction

Hot-wire anemometry is an experimental method for measuring fluid flow, commonly used for unsteady measurements. This method is based on heat convection from the heated wire into the flowing fluid (see, for example, Bruun [1]). The small dimensions of the wires (micrometers in diameter and millimeters in length) ensure that the heat capacity of the heated elements is low. Therefore, rapid changes in the electrical properties can be observed, with frequencies up to hundreds of kHz. The hot-wire anemometers can then be divided into three categories:

1. Constant Current Anemometry (CCA) is a method where a constant current I_w is maintained across the heated element during its operation, resulting in changes of the wire resistance. CCA is simple method, but thanks to the lower frequency responses is less common.

2. Constant Voltage Anemometry (CVA) is a method where a constant voltage $E_\mathrm{w} = I_\mathrm{w} R_\mathrm{w} =$ const. is maintained during the measurement, therefore measurable output is the varying electric current.

3. Constant Temperature Anemometry (CTA) is a method where the constant temperature (which is equivalent to resistance R_w) of the wire is maintained during the anemometer's operation, meaning that the measured variable is the varying anemometer voltage E_w.

The advantage of the CTA regime in hot-wire anemometry is that the temperature variation of the wire is automatically compensated for by the electric circuit during the measurement. Therefore, the thermal inertia of the sensor does not need to be taken into account. In contrast, other methods may require additional signal filtering to compensate for this thermal inertia. Other advantages and disadvantages of these methods can be found in [2]. The detailed introduction into the problem of hot-wire measurement is the work of Jørgensen [3]. There are other detailed studies concerning hot-wire anemometry that were conducted by many research groups around the world, including the group of Prof. Uruba, Dr. Jonáš, and Dr. Mazur in the Czech Republic. See, for example, the work of Jonáš [4] and [5], along with the references cited therein, to name a few.

Accurate data evaluation in hot-wire anemometry relies on several critical parameters, among which the geometry of the wire plays a crucial role , see e.g. Derksen and Azad [6]. The diameter, length, and surface properties of the wire directly influence heat transfer characteristics, introducing dependencies that are often encapsulated in similarity criteria. These criteria, such as the Nusselt and Reynolds numbers, are used to establish relationships between the heat transfer rate, flow regime, and wire properties.

2 Motivation and aim of the work

The first part of this paper focuses on a brief description of the function of hot-wire anemometry to provide background for readers who are not familiar with the method.

The main goal of the paper is the precise estimation of wire dimensions, as these are essential for the proper evaluation of the similarity criteria equation between the Reynolds and Nusselt numbers. According to the authors' knowledge, there is no universal form of such an equation in the current literature. This is because the measurements are affected by many variables (see equation (1)). Some corrections have already been estimated (for example, for the temperature effect), while others have not. The correction for wire length was introduced by Derksen and Azad [6]; however, the aim of their work was to correct spectrum and dissipation errors in pipe boundary layers caused by the large dimensions of the wire compared to the small-scale structures in the flow field.

The purpose of the theoretical calculations is to show that, although the temperature of the wires in operational conditions is set to some average value, the temperature distribution along the wire is not uniform. This non-uniformity can affect the results, as the measured voltages are integral values, and the same finest scales in the flow field will interact differently with different parts of the wire.

Admittedly, at this time, our results will have a slight effect on hot-wire measurements, as individual wires are usually calibrated before each experimental campaign, and the calibration dependencies between fluid velocities and measured voltages are used to calculate the desired flow properties. However, if the l/d correction will be established in future work, the present study will contribute significantly to this effort.

3 Short description of the theory behind the hot-wire anemometry

The general form of the heat transfer from the heated long wire into the flowing fluid is described by the Nusselt number, which is a function of:

$$Nu = Nu\left(Re, M, Gr, Pr, Kn, a_{\mathrm{w}}, \frac{l}{d_{\mathrm{w}}}\right), \tag{1}$$

where M is the Mach number, Re is the Reynolds number, Gr is the Grashoff number, Pr is the Prandtl number, Kn is the Knudsen number, l/d_{w} is the aspect ratio of the wire and a_{w} is the overheat ratio. In experiments conducted in air at low speeds (the incompressible limit), several of these similarity criteria can be ignored, particularly the Mach and Grashoff numbers. The Prandtl number is fixed at Pr=0.7 for air, and the Knudsen number can be neglected due to the continuum hypothesis, therefore:

$$Nu = Nu\left(Re, a_{\mathrm{w}}, \frac{l}{d_{\mathrm{w}}}\right), \tag{2}$$

with the definition of Nusselt and Reynolds numbers:

$$Nu = \frac{R_{\mathrm{w}} I_{\mathrm{w}}^2}{\pi l k \left(T_{\mathrm{w}} - T_{\mathrm{a}}\right)}, \qquad Re = \frac{\varrho U d_{\mathrm{w}}}{\mu}, \tag{3}$$

where R_{w}, I_{w} and T_{w} are the wire resistance, current and, temperature at operational conditions, T_{a} si the ambient temperature, ϱ, U and μ are the fluid density, velocity and dynamic viscosity and d_{w} and l are the wire diameter and length, respectively. The dependencies of these similarity criteria on the wire dimensions are evident from this relationship.

The first study addressing the topic of forced convection from a wire was conducted by King [7]. He obtained the simplest equation relating the measured voltage to fluid velocity in the form of $E = a + b\sqrt{U}$. The more general form of this equation is:

$$Nu = \left(\mathcal{A} + \mathcal{B} Re^n\right)\left(\frac{T_{\mathrm{w}} + T_{\mathrm{a}}}{2}\right)^m = \left(\mathcal{A} + \mathcal{B} Re^n\right) T_{\mathrm{f}}^m, \tag{4}$$

here, $\mathcal{A}$ and $\mathcal{B}$ are referred to as constants. However, these parameters, as well as the exponents n and m, are not truly constants. Their values depend on the flow regime around the cylinder, as well as on the wire geometry and temperature. The variations of these constants can be found in paper written by Andrews et al. [8]. Some of the relevant constants are listed in Table 1 and illustrated in Figure 1.

Table 1: Correlation equations from literature.

Reference	Equation	Validity range Re_f
King [7]	$Nu_\mathrm{f} = 0.318 + 0.690 Re_\mathrm{f}^{0.5}$	$0.055 < Re_\mathrm{f} < 55$
Kramers [9]	$Nu_\mathrm{f} = 0.039 + 0.510 Re_\mathrm{f}^{0.5}$	$0.01 < Re_\mathrm{f} < 10^4$
McAdams [10]	$Nu_\mathrm{f} = 0.32 + 0.430 Re_\mathrm{f}^{0.52}$	$0.01 < Re_\mathrm{f} < 10^3$
Douglas and Churchill [11]	$Nu_\mathrm{f} = 0.00128 Re_\mathrm{f} + 0.460 Re_\mathrm{f}^{0.5}$	$500 < Re_\mathrm{f} < 3 \times 10^5$
Van der Hege Zijen [12]	$Nu_\mathrm{f} = 0.35 + 0.001 Re_\mathrm{f} + 0.50 Re_\mathrm{f}^{0.5}$	$0.01 < Re_\mathrm{f} < 10^4$
Collins and Williams [13]	$Nu_\mathrm{f} = \left(0.24 + 0.56 Re_\mathrm{f}^{0.45}\right) \left(T_\mathrm{f}/T_\mathrm{a}\right)^{0.17}$	$0.02 < Re_\mathrm{f} < 44$
Andrews et al.[8]	$Nu_\mathrm{f} = 0.34 + 0.65 Re_\mathrm{f}^{0.45}$	$0.015 < Re_\mathrm{f} < 20$

The knowledge of the wire dimensions is crucial, as evidenced by the definitions of the similarity criteria in (4), where the diameter and length of the wire are explicitly included. To illustrate their significance, a simple calculation of the temperature distribution along the wire can be performed, as shown by Bruun [1]. The steady-state condition of the system along the wire, neglecting radiation, yields a differential equation of the form:

$$0 = k_\mathrm{w} A_\mathrm{w} \frac{\mathrm{d}^2 T_\mathrm{w}}{\mathrm{d}x^2} + \left(\frac{I^2 \mathcal{R}_0 \alpha_0}{A_\mathrm{w}} - \pi d_\mathrm{w} h\right)(T_\mathrm{w} - T_\mathrm{a}) + \frac{I^2 \mathcal{R}_\mathrm{a}}{A_\mathrm{w}}, \tag{5}$$

where $\mathcal{R}_0$ represents the resistivity of the wire at the temperature T_0 (provided by the manufacturer), and $\mathcal{R}_\mathrm{a}$ is the resistivity of the wire at the ambient temperature. Introducing substitutions:

$$K_1 = \frac{I^2 \mathcal{R}_0 \alpha_0}{k_\mathrm{w} A_\mathrm{w}^2} - \frac{\pi d_\mathrm{w} h}{k_\mathrm{w} A_\mathrm{w}}, \tag{6}$$

$$K_2 = \frac{I^2 \mathcal{R}_\mathrm{a}}{k_w A_\mathrm{w}^2} - \left(\frac{I^2 \mathcal{R}_0 \alpha_0}{k_\mathrm{w} A_\mathrm{w}^2} - \frac{\pi d_\mathrm{w} h}{k_\mathrm{w} A_\mathrm{w}}\right) T_\mathrm{a}, \tag{7}$$

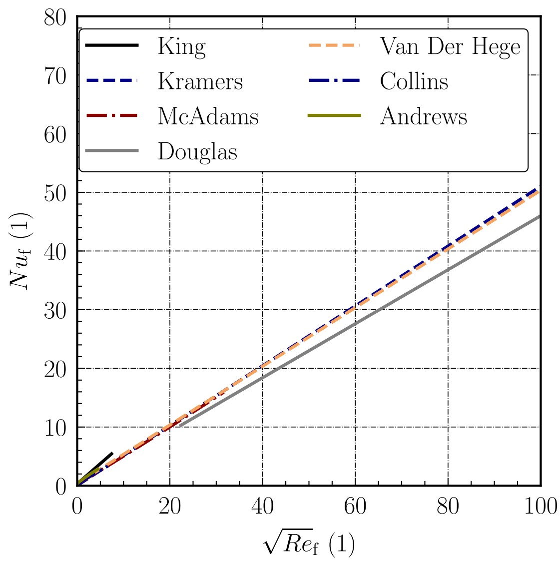

Figure 1: Plot of the dependencies between Nusselt and Reynolds numbers based on equations given in Table 1.

equation (5) can be simplified:

$$\frac{\mathrm{d}^2 T_\mathrm{w}}{\mathrm{d}x^2} + K_1 T_\mathrm{w} + K_2 = 0. \tag{8}$$

Solving this differential equation gives:

$$T_\mathrm{w}(x) = C_1 e^{-x\sqrt{-K_1}} + C_2 e^{x\sqrt{-K_1}} - \frac{K_2}{K_1}. \tag{9}$$

The constants C_1 and C_2 can be obtained from the boundary conditions. In the positions $x = 0$ and $x = l$ temperature has to be equal to T_a, therefore:

$$C_1 = \frac{K_1 T_a e^{l\sqrt{-K_1}}}{K_1 e^{l\sqrt{-K_1}} + K_1} + \frac{K_2 e^{l\sqrt{-K_1}}}{K_1 e^{l\sqrt{-K_1}} + K_1}, \tag{10}$$

$$C_2 = \frac{K_1 T_a}{K_1 e^{l\sqrt{-K_1}} + K_1} + \frac{K_2}{K_1 e^{l\sqrt{-K_1}} + K_1}. \tag{11}$$

Note that constant K_1 can be positive or negative; therefore, absolute values must be taken for the calculation.

4 Used methods

4.1 Electron microscope VEGA II LSH

The electron microscope used was the scanning electron microscope (SEM) VEGA II LSH, as described in [14]. The simplified version of the microscope is shown in Figure 2. The microscope consists of three main parts: the column, where electrons are emitted and prepared for scanning; the chamber, which houses the tested object and detectors; and the vacuum system.

Electrons are emitted from the electron gun, which consists of a cathode made of a heated tungsten filament that emits electrons, and a Wehnelt cylinder with a different potential compared to the cathode. This potential difference accelerates the electrons between the cathode and the cylinder. An anode is placed at the end of the electron gun. Below the gun, a gun-centering mechanism ensures that the electron beam remains straight. Slightly lower, a spray aperture is positioned to cut off the outer part of the electron beam. This is followed by two condensers that serve as magnetic lenses. A fixed aperture with a diameter of approximately 50 µm is included to optimize the final size of the electron beam. Next, an auxiliary lens is present, serving as a preparatory device for the electron beam before it reaches the stigmator, which compensates for astigmatism, and the final lens, which focuses the beam onto the studied object.Between the stigmator and the final lens, two scanning coils are present. These coils serve to amplify the beam and enable its precise shifting, if needed.

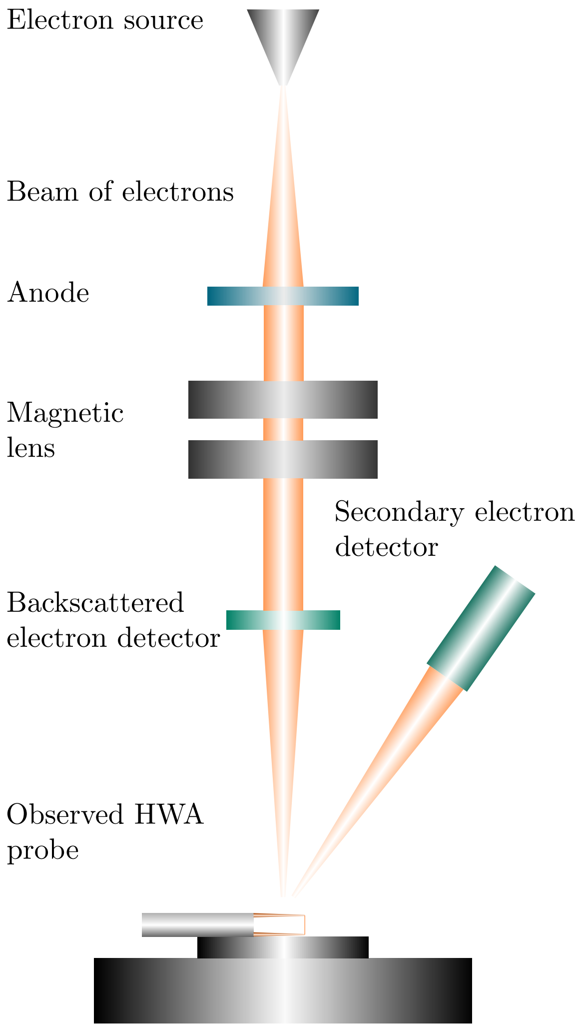

Figure 2: Scheme of the SEM electron microscope.

The next part is the vacuum chamber beneath the column, where the object being studied is placed. The sample can be moved both horizontally and vertically, as well as rotated, in this type of microscope. The detector detects the secondary electrons that are emitted from the surface of the object due to interaction with the primary electron beam. These low-energy electrons are first accelerated in the detector and focused onto a scintillator. They are then detected outside the microscope by a photomultiplier.

4.2 Measurement of the wire dimensions

The measurements of the wire diameter and length were straightforward. The photographs captured using the electron microscope were uploaded into Python, where three steps were performed:

1. First, the reference dimension from the scale in the image, generated by the EM control software, was established.
2. The second step was to measure the required dimension of the wires. This was done multiple times and at several positions along the wire.
3. The final step was to average these measured values to reduce the error in the process.

Regarding the uncertainty of the measurements, it arises from both the resolution of the photographs and the measurement process itself. The resolution of the photographs was 1536 × 1536 pixels. For example, the scale for a magnification of 22.5 $\times 10^3$ has a length of 400 pixels, which corresponds to 5 μm, i.e. that 1 pixel represents a distance of 12.5 nm. Based on several measurements, the error in determining the wire diameter was less than 10 pixels, or 0.125 μm. The measurements were performed manually by selecting two points across the wire and calculating their distance. This approach introduces an error that tends to overestimate the measured values.

5 Results and discussions

Six single-wire Dantec probes 55P11, were investigated using an electron microscope. These probes are named as S2, S3, S6, S7, S13, and S18. All of the probes were photographed at two magnifications: the first, lower magnification was used to measure the length of the wires, while the second, higher magnification was used to measure the wire diameters. The purpose of this investigation was to compare the actual dimensions of the wires with those provided by the manufacturer. According to the specifications, the diameter of the wire should be $d_{\mathrm{given}} = 5$ μm, and the length of the wires between the prongs should be $l_{\mathrm{given}} = 1.2$ mm, according to Dantec specification.

Probes S6, S7, and S13 were, however, damaged during the experiments and repaired prior to this study. Therefore, it was also desirable to check the quality of the repairs. The other probes, S2, S3, and S18, were in their original condition, and the dimensions of their wires were checked to establish the precision of the manufacturer.

It can be seen that the probes S2, S3, and S18 (Figures 3a - 3e and Figures 3i - 3l), in their original condition, were nicely stretched between the prong tips. The solder joints were small, and therefore, the heat transfer in the prong regions to the surroundings should be minimized as much as possible.

On the other hand, the repaired probes S6, S7, and S13 (Figures 3c - 3k) exhibit different geometrical characteristics. Starting with probe S13, the wire was nicely stretched between the prongs but extended significantly over one of the prongs. Moreover, it is evident that the wire was used in an environment with some oil suspension, as indicated by the 'bubbles' observed in Figure 3k. The other two probes (S6 and S7) were repaired and used in a clean environment and, therefore, were not contaminated by oil like probe S13. However, it was found that during the repair, the wires were not sufficiently stretched between the prongs and that the wires were bent. Such bending could affect the basic measurement results, such as the Nusselt-Reynolds relationships.

The calculation using dimensions obtained from the EM measurements was performed for the ambient temperature $T_{\mathrm{a}} = 300$ K and overheat ratio $a_{\mathrm{w}} = 0.8$.

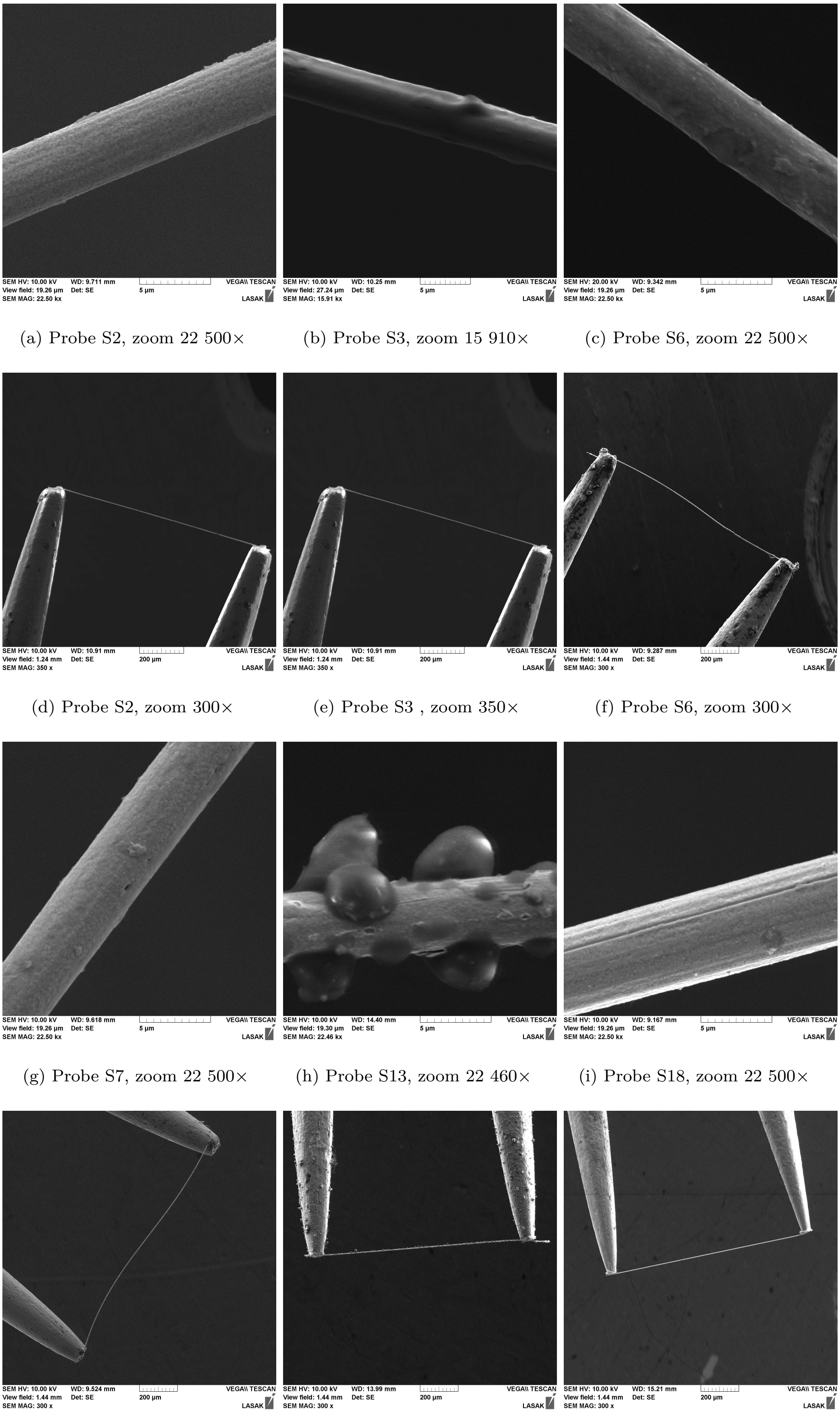

(a) Probe S2, zoom 22 500×
(b) Probe S3, zoom 15 910×
(c) Probe S6, zoom 22 500×
(d) Probe S2, zoom 300×
(e) Probe S3 , zoom 350×
(f) Probe S6, zoom 300×
(g) Probe S7, zoom 22 500×
(h) Probe S13, zoom 22 460×
(i) Probe S18, zoom 22 500×
(j) Probe S7, zoom 300×
(k) Probe S13 , zoom 300×
(l) Probe S18, zoom 300×

Figure 3: Hot-wire probes photographed under electron microscope.

To obtain dimensionless distribution of the temperature along the wire, integral value of the temperature of the wire is introduced as:

$$T_{\text{int}} = \frac{1}{l}\int_{0}^{l} T_{\text{w}}(x)\mathrm{d}x. \tag{12}$$

Other parameters used in the equation (9), i.e. material parameters, were taken from [2] for tungsten. The electric properties were obtained from the measurements with the individual wires in VZLU laboratory of high speed aerodynamic.

Dimensions of the wires of the probes measured from the figures are summarized in Table 2. The values introduced in this table are defined as follows:

$$\Delta d_{\text{w}} = \frac{d_{\text{given}} - d_{\text{w}}}{d_{\text{given}}} \qquad \longrightarrow \qquad d_{\text{given}} = 5\ \mu\text{m}, \tag{13}$$

$$\Delta l_{\text{mean}} = \frac{l_{\text{given}} - \frac{l_{\text{in}}+l_{\text{out}}}{2}}{l_{\text{given}}} \qquad \longrightarrow \qquad l_{\text{given}} = 1.2\ \text{mm}. \tag{14}$$

Table 2: Dimensions of the tested wires:

probe	d_{w} (μm)	Δd_{w} (1)	$\sigma_{d_{\text{w}}}$ (%)	l_{in} (mm)	l_{out} (mm)	Δl_{mean} (1)	$\sigma_{l_{\text{w}}}$ (%)
s2	4.87	0.026	3.09	1.160	1.512	-0.069	0.53
s3	4.65	0.070	4.58	0.887	1.069	0.218	0.62
s6	4.76	0.048	3.16	0.998	1.177	0.130	0.65
s7	4.71	0.058	3.19	1.267	1.398	-0.066	0.53
s13	4.98	0.004	3.02	1.049	1.191	0.104	0.63
s18	6.28	-0.256	2.40	1.017	1.100	0.153	0.67

The temperature distribution along the tested wires for the tested probes is shown in Figure 4. It is evident that shorter wires have a larger area affected by heat transfer into the prongs. For the shortest wire (S3), approximately 40% of the wire length remains unaffected. In contrast, for probe S7, this unaffected region extends to about 60%.

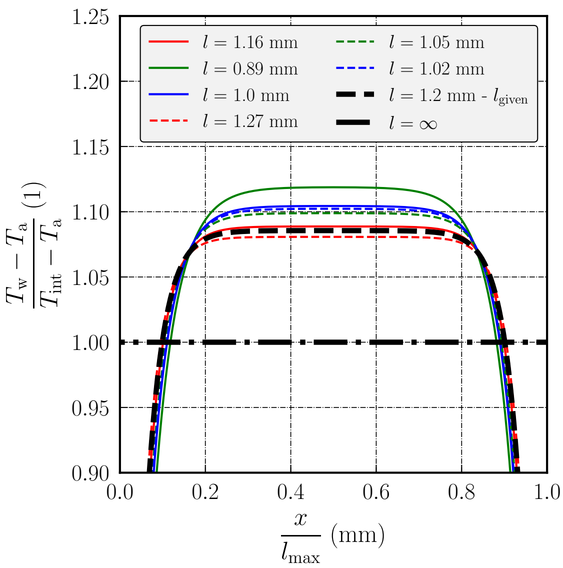

Figure 4: Theoretical temperature distributions for tested hot-wire probes.

6 Conclusion

The presented paper focuses on the visualization of Dantec hot-wire probes (55P11) under an electron microscope. The dimensions of the probes, specifically their diameter and length, were evaluated and used to calculate the temperature distribution along the individual investigated probes. This analysis highlights the importance of accurately determining these parameters. It was demonstrated that the measured dimensions differed significantly from the manufacturer-provided specifications, with deviations of up to 25.6% in diameter for probe S18 and 21.8% in length for probe S3. The obtained data will be utilized in future work to determine the effect of these parameters on the calibration of the probes and the coefficients in equation (4). It is important to note that the dimensions are not the only critical parameters influencing the evaluation; other factors, such as the temperature of the flowing fluid, the effect of compressibility, and additional variables, must also be considered.

Declaration

The spell check was performed using ChatGPT 3.5.

Acknowledgment

The authors would like to express gratitude to LASAK s.r.o. for their support in providing the electron microscope used for the experiments presented in this contribution.

References

[1] Bruun H.H.:Hot-Wire Anemometry Principles and Signals Analysis. Oxford university press, (1995)

[2] Eds. Tropea C., Larin A.J., Foss J.F.: Handbook of Experimental Fluid Mechanics. Springer, (2007)

[3] Jørgensen F.E.: How to measure turbulence with hot-wire anemometers - a practical guide, Dantec Dynamics, (2005)

[4] Jonáš P.: Properties and Development of Turbulent Flows Under the Influence of Significant Effects for Internal Aerodynamics, *Doctoral thesis*, (1991), in Czech.

[5] Jonáš P.: Rotary slanted single wire CTA - a useful tool for 3D flows investigations, *EPJ Web of Conferences*, Vol. 45, (2013)

[6] Derksen R. W., Azad R. S.: An Examination of Hot-Wire Corrections, *Phys. Fluids*, vol. 26, pp. 1751 - 1754, (1983)

[7] King L.V.: On the Convective Heat Transfer from Small Cylinders in a Stream of Fluid, Determination of Convective Constants of Small Platinum Wires with Application to Hot-Wire Anemometry. In: *Proceedings of the Royal Society of London. Series A, Containing Papers of a Mathematical and Physical Character*, pp. 563–570, (1914)

[8] Andrews G. D., Bradley, and G. Hundy. Hot Wire Anemometer Calibration for Measurement of Small Gas Velocities. *Int. J. Heat Mass Trasnfer* vol. 15, pp. 1765–1786, (1972)

[9] Kramers, H.: Heat transfer from spheres to flowing media. In: *Physica*, vol. 12, pp. 61–80, (1964)

[10] McAdams, W.: Heat Transmission. McGraw-Hill, New York, (1954)

[11] Douglas W., S. Churchill.: Recorrelation of data for convective heat transfer between gases and and single cylinders with large temperature differences. In: *Chem. Engng Prog. Symp.*, pp. 23–28, (1956)

[12] Van der Hege Zijen, B.: Modified Correlation Formulae for the Heat Transfer by Natural and Forced Convection from Horizontal Cylinders. In: *Appl. Sci. Res* vol. 6, pp. 129–140, (1956)

[13] Collins D., M. Williams.: Two-dimensional Convection from Heated Wires at Low Reynolds Numbers. In: *J. Fluid Mech.* vol. 6, pp. 357–384, (1959)

[14] Scanning Electron Microscope VEGA II LSH instruction for use, TESCAN, s.r.o., `https://engineering.tamu.edu/mechanical/_files/_documents/_content-documents/VEGA_II_Manual-eng-.pdf`, access (11. 12. 2024)